The oxygenated products of cryptotanshinone by biotransformation with *Cunninghamella elegans* exerting anti-neuroinflammatory effects by inhibiting TLR 4-mediated MAPK signaling pathway

Jing-Shuai Wu
Ocean University of China
Qin-Yu Meng
Ocean University of China
Xiao-Hui Shi
Ocean University of China
Zhen-Kun Zhang
Ocean University of China
Hua-Shi Guan
Ocean University of China
Chang-Lun Shao
Ocean University of China
Chang-Yun Wang (changyun@ouc.edu.cn)

Research

Keywords: Salvia miltiorrhiza Bunge, cryptotanshinone, biotransformation, Cunninghamella elegans, anti-neuroinflammatory.

Posted Date: March 26th, 2020

DOI: https://doi.org/10.21203/rs.3.rs-19324/v1

Version of Record: A version of this preprint was published at Bioorganic Chemistry on November 1st, 2020. See the published version at https://doi.org/10.1016/j.bioorg.2020.104246.

Abstract

Background: Neuroinflammatory processes are critical in the development and progression of Alzheimer's disease (AD). The potent anti-neuroinflammatory inhibitors are expected as the candidates to treat AD. Cryptotanshinone (**1**), a major bioactive constituent in the traditional Chinese medicinal herb Dan-Shen *Salvia miltiorrhiza* Bunge, has been reported to possess remarkable pharmacological activities, especially anti-oxidation and anti-inflammation.

Methods: Cryptotanshinone (**1**) was biotransformed with the fungus *Cunninghamella elegans* AS3.2028 to improve its bioactivities and physicochemical properties. The structures of transformed products were elucidated by comprehensive spectroscopic analysis including HRESIMS, NMR and ECD data. Their anti-neuroinflammatory activities were assessed by ELISA, transcriptome analysis, western blot, and immunofluorescence methods.

Results: Three oxygenated products (**2**–**4**) at C-3 of cryptotanshinone (**1**) were obtained, among them **2** was a new compound. All of the biotransformed products (**2**–**4**) were found to inhibit significantly lipopolysaccharide-induced nitric oxide production in BV2 microglia cells with the IC_{50} values of 0.16–1.16 μM, approximately 2–20 folds stronger than the substrate (**1**). These biotransformed products also displayed remarkably improved inhibitory effects on the production of inflammatory cytokines (IL-1β, IL-6, TNF-α, COX-2 and iNOS) in BV-2 cells via targeting TLR4 compared to substrate (**1**). The underlying mechanism of **2** was elucidated by comparative transcriptome analysis, which suggested that it reduced neuroinflammatory mainly through mitogen-activated protein kinase (MAPK) signaling pathway. Western blotting results revealed that **2** downregulated LPS-induced phosphorylation of JNK, ERK, and p38 in MAPK signaling pathway.

Conclusion: The biotransformed products of cryptotanshinone exhibit potent anti-neuroinflammatory activities. These findings provide a basal material for the discovery of candidates in treating AD.

1. Introduction

Alzheimer's disease (AD) is a progressive and irreversible neurodegenerative disorder and the most common form of dementia among the elderly[1]. The multiple mechanisms about its occurrence and development have been revealed[2]. Many therapeutic approaches and clinic trials to AD have been reported[3]. Until 2018, only five small molecular chemicals are used clinically as drugs for the treatment of AD[3]. In 2019, one sodium oligomannate derived from a traditional Chinese medicine seaweed, GV-971, was approved as a drug in China to relieve AD by inhibiting β-amyloid protein aggregation, remodeling gut microbiota and suppressing gut bacterial amino acids-shaped neuroinflammation[4]. It should be noted that neuroinflammatory processes are critical in the development and progression of AD[5–8]. Therefore, the potent anti-neuroinflammatory inhibitors derived from natural products are expected as the candidates to treat AD[9].

Tanshinones are a class of lipophilic abietane diterpenes mainly isolated from Dan-Shen Salvia miltiorrhiza Bunge which is a well-known traditional Chinese medicine[10]. Modern pharmacological studies have demonstrated that tanshinones possess a variety of bioactivities, such as anti-inflammatory, anti-oxidative, acetylcholinesterase inhibitory, β-amyloid protein aggregation inhibitory, and neuroprotective activities[11,12]. These tanshinones from S. miltiorrhiza have shown an exciting prospect for the treatment of AD[13,14]. Among the tanshinones, sodium tanshinone IIA sulfonate has been developed successfully as a clinically effective drug to treat angina pectoris and coronary artery disease[12]. It has attracted extensive attentions that cryptotanshinone, another representative bioactive component in tanshinones, has been proved to be a promising candidate to treat AD[15,16]. However, the poor water solubility of cryptotanshinone limits its bioavailability and possible clinical applications[16,17]. Under the above considerations, it is urgent to discover cryptotanshinone derivatives featuring better bioavailabilities with high activities.

A literature survey revealed that cryptotanshinone has been remoulded to obtain modified derivatives by chemical and biological approaches[14,18–21]. Compared to chemical approaches, biotransformation of cryptotanshinone has proven to be an attractive alternative to improve the physicochemical and pharmacological properties. For example, five anhydrides of cryptotanshinone with anti-influenza A virus activities were obtained via biotransformation by fungus Mucor rouxii[20]. Three oxygenated products were harvested under the action of fungus Cunninghamella elegans in a gentle manner without changing the skeleton of ortho-naphthoquinone of cryptotanshinone[21]. It should be noted that the fungal genus Cunninghamella could be used as a microbial model to mimic mammalian drug biotransformation and as an in vitro model for drug metabolism studies[22]. It has been reported that C. elegans could be used as an in vitro model for the achievement of the in vivo minor metabolites of cryptotanshinone[21,23].

In the present work, cryptotanshinone (1) was biotransformed using the fungus C. elegans AS3.2028 to obtain its new derivatives with improved physicochemical properties and bioactivities. As a result, multiple transformed products of cryptotanshinone have been emerged in the fermentation broth in 72 h. Three metabolites (2 – 4) (Fig. 1) have been isolated and characterized from the biotransformed products. The metabolite 2, (15R)-3-keto-cryptotanshinone, was found to exhibit potential anti-neuroinflammatory activity, representing a promising candidate for the discovery of AD drugs. Herein, we report the biotransformation of cryptotanshinone (1), and the isolation, structure elucidation, biological evaluation and preliminary mechanism interpretation of the biotransformed products.

2. Materials And Methods

2.1. Materials

Optical rotations were measured on a JASCO P-1020 digital polarimeter. UV spectra were recorded on a HITACHI UH 5300 UV spectrophotometer. ECD data were acquired on a J-815-150S Circular Dichroism spectrometer. IR spectra were recorded on a Nicolet-Nexus-470 spectrometer using KBr pellets. ^{1}H and ^{13}C

NMR spectra were acquired by a JEOL Eclips-500 spectrometer at 500 MHz for ^{1}H and 125 MHz for ^{13}C in $CDCl_3$, using TMS as internal standard. HREIMS were measured on a Thermo MAT95XP high resolution mass spectrometer, and EIMS spectra on a Thermo DSQ Elmass spectrometer. Semi-preparative HPLC was performed on a Hitachi L-2000 HPLC system coupled with a Hitachi L-2455 photodiode array detector and using a semi-preparative C_{18} column (Kromasil 250 × 10 mm, 5 μm). The column temperature was set at 30 °C, and the flow rate was 2 mL/min. Silica gel (Qing Dao Hai Yang Chemical Group Co.; 300 − 400 mesh) was used for column chromatography (CC). Precoated silica gel plates (Yan Tai Zi Fu Chemical Group Co.; G60, F-254) were used for thin-layer chromatography. LPS from Escherichia coli O111:B4 and AChE from Electrophorus electricus were purchased from Sigma (Sigma-Aldrich, USA). Primary antibodies against COX-2 (#12282), iNOS (#13120), TLR4 (#14358), p38 (#8690), ERK (#4695), JNK (#9252), phosphor-ERK1/2 (Thr202/Tyr204, #4370), phosphor-p38 (Thr180/Tyr182, #4511), phosphor-JNK (Thr183/Tyr185, #4668) and NF-κB p65 (#8242) were purchased from Cell Signaling Technology (Beverly, MA, USA).

2.2. Substrate

Cryptotanshinone (1) was purchased from Macklin Biochemical Co., Ltd in Shanghai, China and authenticated by comparing its physical and spectroscopic data with the reported values. Its purity was determined to be 98% by HPLC analysis.

2.3. Fungal Strain

The fungus C. elegans AS3.2028 was purchased from China General Microbiological Culture Collection Center, Beijing, China.

2.4. Biotransformation Medium

The biotransformation experiment was carried out in modified Czapek–Dox medium, which consisted of the following ingredients: glucose (15 g/L), sucrose (15 g/L), $MgSO_4 \cdot 7H_2O$ (0.5 g/L), $K_2HPO_4 \cdot 3H_2O$ (1 g/L), $FeSO_4 \cdot 7H_2O$ (0.01 g/L), peptone (5 g/L), KCl (0.5 g/L) and distilled water.

2.5. Biotransformation Procedure

A spore suspension of the fungus grown on PDA was transferred to 500 mL Erlenmeyer flasks containing 100 mL biotransformation medium, and incubated at 28 °C, 180 rpm on a rotary shaker for 24 h. Subsequently, the substrate cryptotanshinone (1) dissolved in methanol was added to each flask to achieve a final concentration of 0.1 mg/mL in a sterile condition. The cultures were incubated for another 72 h.

2.6. Extraction and Isolation

The large-scale cultures (10 L) were filtered and the filtrate was extracted with an equivalent volume of EtOAc for three times. The organic layer was collected and concentrated under vacuum at 40 °C. The EtOAc extract was subjected to silica gel CC eluted with petroleum ether − acetone (10:1 to 1:4) to give

five fractions (Fr.1 – Fr.5). Fr.4 was subjected to semi-preparative HPLC (MeOH – H_2O, 55%) to provide metabolites 2 (6.2 mg), 3 (56.0 mg), and 4 (17.8 mg).

(15R)-3-keto-cryptotanshinone (2)

red powder; [α] $^{20}_{D}$ −33.9 (c 0.05, MeOH); UV (MeOH) λ_{max} (log ε) 209 (1.47), 264 (0.93) nm; IR (KBr) ν_{max} 3741, 3445, 1645, 1558 cm^{-1}; ^{1}H NMR (500 MHz, $CDCl_3$) and ^{13}C NMR (125 MHz, $CDCl_3$), see Table 1; HRESIMS m/z 311.1273 $[M + H]^+$ (calcd for $C_{19}H_{19}O_4$, 311.1278).

2.7. Bioassay for NO Production Inhibitory Activities

The bioassay for NO production inhibitory activities was performed as described by Xia et al.[24]. The BV-2 microglia cells were seeded in 96-well plates. In each well, LPS (1 μg/mL) was added after treating with or without compounds at various concentrations for 24 h. The NO production in the supernatant was detected by the Griess reaction. The absorbance at 540 nm was measured in a microplate reader. The NO concentration and the inhibitory rate were calculated through a calibration curve. Quercetin was used as the positive control. Experiments were operated in triplicate, and the data were described as mean ± SD of three independent experiments.

2.8. ELISA Measurement

The BV-2 microglial cells were cultured in 96-well plates, grown overnight, incubated with compounds for 1 h, and then stimulated with LPS (1 μg/mL) for 24 h. The supernatant (50 μL) from the culture was collected to determine the concentrations of IL-6, IL-1β and TNF-α with ELISA kits according to the protocols.

2.9. Western blot

BV-2 cells were seeded in 6-well plates, incubated with or without compounds for 1 h, then treated with or without LPS (1 μg/mL) for 16 h. The cells were lysed with RIPA lysis buffer. The concentrations of protein were determined by Pierce Rapid Gold BCA Protein Assay Kit. The quantified protein of each sample was electrophoresed in 10% SDS-PAGE, and then transferred to a polyvinylidene difluoride (PVDF) western membrane. The membranes were blocked using 5% (W/V) skim milk in TBST (Trisbuffered saline with 0.1% Tween 20) for 2 h. Then the membranes were incubated with primary antibodies at 4 °C overnight. After being washed by TBST three times, the membranes were incubated with corresponding secondary antibody at room temperature for 2 h. Finally, immunoreactive signals were detected using a chemiluminescence imager (GE Amersham Imager 600, USA). Intensities of band signals were quantified using the densitometric ImageJ software (National Institutes of Health, MD).

2.10. Transcriptome sequencing

The BV-2 cells were treated with 10 μM of compound 2 (sample group) or DMSO (model group) for 1 h followed by stimulated with LPS (1 μg/mL) for 24 h. The control group was without LPS stimulation. Total RNAs were extracted with Trizol (Invitrogen, USA) from the treated BV-2 cells. Three biological

replicates were sequenced using the Illumina Hiseq × 10 platform for each group. The differentially expressed genes (DEGs) were screened out with a q value (p-adjust value) ≤ 0.01 and fold change ≥ 2 and further analyzed with KEGG.

2.11. Cell Viability Assay

The mouse hippocampal neuron cell line (HT22) was used in glutamate toxicity model to evaluate the neuroprotective activities of compounds[25]. The HT22 cells were cultured in 96-well plates and pretreated with tested compounds (1 μM and 0.1 μM) for 1 h. To each well, 5 mM glutamate was added. After treatment for 12 h, the culture medium was replaced with 3-(4,5-dimethylthiazol-2-yl)-2,5-diphenyl tetrazolium bromide (MTT) solution (0.5 mg/ml) and incubated in the dark at 37 °C for 4 h. The MTT solution was carefully removed. Dimethyl sulfoxide was added to dissolve the formazan crystals. The absorbance was detected at 540 nm using a microplate reader. Experiments were operated in triplicate. The cell survival rates to vehicle were calculated with Graphpad prism 7.

For BV-2 cells, after being seeded into a plate, the cells were incubated with various concentrations of the compounds for 24 h. The MTT assay was used to evaluate their cytotoxic activities, consistent with the above operations.

2.12. Immunofluorescence Assay.

The immunofluorescence assay was performed as described by Xia et al.[24]. Briefly, BV-2 cells were pre-treated with DMSO, LPS, and 10 μM compound 2 before LPS, respectively. The cell-seeded glass coverslips were subjected to treatment with cold 4% paraformaldehyde and 0.2% Triton X-100 (in PBS). Then, the coverslips were blocked with 5% BSA (in PBS) for 1 h and incubated with a primary antibody NF-κB p65 at 4 °C overnight, followed by addition of a secondary antibody labeled with Alexa Fluor 594 for 1 h. After being stained with DAPI, the coverslips were washed and sealed. Images were obtained by fluorescence microscope (Leica, Solms, Germany).

2.13. Bioassay for AChE Inhibitory Activities

The AChE inhibitory activities of compounds were evaluated in 96 well microplates using a spectrophotometric method[26,27]. The inhibition rates were calculated by comparing the rates of enzyme reaction of samples relative to that of blank (DMSO). Huperzine A was used as a positive control. All experiments were performed in triplicates independently.

2.14. Physicochemical Properties of Compounds Predicted in silico

The prediction of physicochemical properties, including the number of H-bond donor (HBD) and H-bond acceptor (HBA), 1-octanol/water (Log P), and water solubility (Log S), was conducted using PhysChem Module software in ACD/Labs Percepta 14.0.0[28].

3. Results

3.1. Biotransformation of Cryptotanshinone

In the biotransformation experiments, the substrate, cryptotanshinone (1), was added into the medium with the fungus C. elegans AS3.2028 and incubated at 28 °C, 180 rpm, for 72 h on a rotary shaker. The EtOAc extract of the broth was subjected to the silica gel column chromatography and semi-preparative HPLC, resulting in the isolation of three biotransformed products (2 – 4), of which 2 was a new metabolite.

Metabolite 2 was obtained as a red powder. Its molecular formula was assigned as $C_{19}H_{18}O_4$ based on the $[M + H]^+$ ion peak in HRESIMS with 11 degrees of unsaturation, suggesting the introduction of one oxygen but less two hydrogens than the substrate cryptotanshinone (1). In the ^1H NMR spectrum, two aromatic protons (δ_H 7.62 and δ_H 7.65), one methine, three methylenes (one oxygenated), and three methyl groups were observed (Table 1). The ^{13}C NMR spectrum indicated the presence of 19 carbons, including three ketone carbonyls, eight aromatic carbons (two protonated and six quaternary), one quaternary carbon, one methine, three methylenes (one oxygenated) and three methyl groups (Table 1). These spectroscopic features of 2 were very similar to those of 1. The significant difference was that a ketone carbonyl signal at δ_C 212.5 was presented in 2, by concomitant disappearance of a methylene signal compared to 1 (δ_H 1.66 (2H, m) and δ_C 37.8). The HMBC correlations of 2 from H-1/H-18/H-19 to C-3 indicated that the ketone carbonyl was anchored at C-3. The absolute configuration of C-15 was determined as R by comparison of the experimental and calculated electronic circular dichroism (ECD) curves generated by time-dependent density functional theory (TDDFT) at the B3LYP/6-31G(d,p) level (Fig. 2). Thus, the structure of 2 was characterized as (15R)-3-keto-cryptotanshinone.

Table 1

^{1}H (500 MHz) and ^{13}C (125 MHz) NMR spectroscopic data of metabolite 2 in $CDCl_3$

Position	δ_C, type	δ_H (J in Hz)	Key HMBC
1	25.9, CH_2	3.67, m	C-3, C-5, C-9
2	36.3, CH_2	2.65, m	C-4, C-10
3	212.5, C		
4	48.5, C		
5	150.3, C		
6	131.8, CH	7.65, d (8.1)	C-4, C-8, C-10
7	123.8, CH	7.62, d (8.1)	C-9, C-14
8	126.9, C		
9	128.4, C		
10	141.6, C		
11	184.4, C		
12	175.6, C		
13	119.0, C		
14	170.2, C		
15	34.7, CH	3.63, m	
16	81.6, CH_2	4.41, dd (9.6, 6.1) 4.93, d (9.6)	
17	18.8, CH_3	1.38, d (6.1)	
18	27.0, CH_3	1.48, s	C-3, C-5
19	27.1, CH_3	1.47, s	C-3, C-5

Metabolites 3 and 4 were identified as (3S,15R)-3-hydroxy-cryptotanshinone and (3R,15R)-3-hydroxy-cryptotanshinone, respectively, by comparison of their spectroscopic data with the reported in literature[21]. These two metabolites were two known biotransformed products of cryptotanshinone by using C. elegans AS3.2028[21], the same fungus as we used.

3.2. The Inhibitory Effects of Compounds on the Production of NO, IL-1β, IL-6 and TNF-α in LPS-Induced BV2 Microglia Cells

Nitric oxide, a signaling molecule, plays a key role in the development and progression of inflammation. Inhibitors of NO production represent the potential therapeutic agents for inflammatory diseases[29]. Cryptotanshinone (1) has been reported to possess potent anti-inflammatory activities[30–33]. In the present study, the substrate (1) and its metabolites (2 – 4) were evaluated for their anti-neuroinflammatory activities. All of the compounds showed potent inhibitory activities against lipopolysaccharide (LPS)-induced NO production in BV2 microglia cells (Table 2). The substrate (1) showed better activity with the IC_{50} value of 3.30 μM, approximately 2.5 folds than that of the positive control quercetin (8.50 μM). Compared to 1, metabolites 2 – 4 exhibited improved inhibitory activities against NO production in BV2 cells with the IC_{50} values of 0.49, 1.16, and 0.16 μM, about 6.7, 2.8 and 20.6 folds more potent than 1, respectively. It is also interesting to observe that metabolites 3 and 4, featuring respective β- and α-orientation hydroxyl groups at C-3, exhibited significantly discriminating activities, the latter displaying 7 folds higher activity than the former. It indicated that the oxygenated group at C-3, hydroxyl or carbonyl, might be beneficial to improve the anti-neuroinflammatory activity of cryptotanshinone.

Table 2
Inhibitory effects of compounds 1 – 4 on NO, IL-1β, IL-6, and TNF-α release in BV-2 Cells

Compds.	IC_{50} for NO	IC_{50} for IL-1β	IC_{50} for IL-6	IC_{50} for TNF-α
1	3.30 ± 0.26	5.71 ± 0.21	13.4 ± 0.12	10.02 ± 0.16
2	0.49 ± 0.17	1.34 ± 0.21	9.17 ± 0.17	8.17 ± 0.23
3	1.16 ± 0.15	3.50 ± 0.16	14.75 ± 0.20	9.31 ± 0.13
4	0.16 ± 0.11	2.79 ± 0.22	12.54 ± 0.13	8.45 ± 0.12
Quercetin	8.50 ± 0.35	–	–	–

NO levels in culture supernatants were measured using the Griess reagent, and IL-1β, IL-6, and TNF-α in culture supernatants were determined with an ELISA kit. Values were given as the mean ± SD (μM) from three independent experiments.

The overproduction of pro-inflammatory cytokines in nerve cells usually reflects the activated stress state of cell[34]. The pro-inflammatory cytokines IL-1β, IL-6 and TNF-α in the culture supernatant of LPS-induced BV-2 cells were evaluated by ELISA method. All of the tested compounds (1 – 4) showed remarkable inhibitory effects on the release of IL-1β, IL-6 and TNF-α (Table 2). In comparison to substrate 1, the biotransformed products 2 – 4 showed significantly improved inhibitory effects especially for IL-1β with 4.3, 1.6 and 2.0 folds, respectively. In addition, to exclude the influence of cytotoxicity of compounds to their inhibitory activities, a cytotoxicity assay was conducted against BV-2 cells. As a result, all compounds showed no cytotoxicity at the concentration of 10 μM. Based on the above results, it was confirmed that cryptotanshinone (1) and its metabolites (2 – 4) exhibited anti-neuroinflammatory activities in BV2 cells.

3.3. The Inhibitory Effects of Expressions of iNOS, COX-2, and TLR4 in LPS-Induced BV-2 Cells

In order to further interpret the anti-neuroinflammatory effects of the compounds, the production of two inflammatory mediators in LPS-induced BV-2 cells, iNOS and COX-2, was assayed by western blot. Compared to 1, compounds 2 − 4 exhibited improved inhibitory effects on the level of expressed proteins (Fig. 3). Consequently, the initial inflammatory target TLR4 was detected, which plays an important role in the immune and inflammation system to recognize LPS[35]. BV-2 cells were pretreated with compounds for 1 h and then exposed to LPS for 16 h. As a result, the expression of TLR4 was stimulated by LPS, while cryptotanshinone (1) and its metabolites (2 − 4) reduced its expression level (Fig. 3). Compared to 1, compounds 2 and 4 showed significantly improved effects on inhibiting the expression of TLR4.

3.4. The Targeted Signal Pathway of Compound 2 in LPS-Induced BV-2 Cells

RNA-seq was used to investigate the gene expression profiles of BV-2 cells. It was found that LPS upregulated 1212 genes in the transcript profiles of BV-2 cells, while compound 2 downregulated 306 genes of them (FC ≥ 2-fold change, q value ≤ 0.01) (Fig. 4a and Table S1). The Kyoto Encyclopedia of Genes and Genomes (KEGG) pathway analysis revealed that these differential expressed genes were significantly enriched in the mitogen-activated protein kinase (MAPK) signaling pathway (Fig. 4b). Subsequently, the phosphorylation levels of c-Jun NH_2-terminal protein kinase (JNK), extracellular regulated protein kinases (ERK), and p38 in MAPK signaling pathway were determined with western blot. Compound 2 was founded to inhibit significantly the phosphorylation of JNK, ERK, and p38 with a dose-depend manner (Fig. 5). These findings suggested its potential use to attenuate neuroinflammatory through MAPK signaling pathway. The phosphorylation of JNK, ERK, and p38 usually lead to the activation of NF-κB in nucleus. As expected, compound 2 was also found to reduce the effect of p65 in LPS-stimulated BV-2 cells (Fig. 6), which activated the production of pro-inflammatory cytokines.

3.5. The Neuroprotective Activities of Compounds against HT22 Neuronal Cells

Glutamate is an endogenous excitatory neurotransmitter. Glutamate toxicity has been used as a common model to investigate oxidative stress-induced neuronal cell death[36,37]. Extracellular glutamate with a high concentration could deplete glutathione (GSH) and accumulate reactive oxygen species (ROS) in neurons, which may lead to cell death[38]. In our study, the substrate cryptotanshinone and its converted products were evaluated for their neuroprotective activities against glutamate-induced oxidative toxicity in HT22 neuronal cells. As shown in Fig. 7, cryptotanshinone (1) and its metabolites (2 − 4) could maintain normal cell morphology and significantly attenuated glutamate-induced cytotoxicity in HT22 neuronal cells. The cell viabilities achieved by the metabolites and substrate were more than 90% and 50% at the concentrations of 1 μM and 0.1 μM, respectively.

3.6. The AChE Inhibitory Activities of Compounds

Acetylcholinesterase (AChE, 3.1.1.7) can catalyze the hydrolysis of choline esters and act in cholinergic neurotransmission by breaking down acetylcholine (ACh), a cholinergic neurotransmitter. Reduced cholinergic neuron activity is one of the recognized features of AD[39]. The inhibitors of AChE are potential to restore the normal ACh level to relieve AD. In our study, the acetylcholinesterase inhibitory activities of cryptotanshinone and its converted products were evaluated. The results showed that cryptotanshinone (1) had a weak acetylcholinesterase inhibitory activity (IC_{50} = 214.52 μM) against AChE from Electrophorus electricus. Among the three metabolites, only 2 exhibited obviously improved AChE inhibitory activity (IC_{50} = 23.84 μM), nearly 9 folds more potent than the substrate (1).

3.7. Physicochemical Properties of Compounds Predicted in silico

The physicochemical properties of tanshinones are critical to their bioavailabilities in vivo[11]. The physicochemical properties of the metabolites of cryptotanshinone (1) were predicted by using the ACD/Labs Percepta platform-PhysChem Module software. The substrate cryptotanshinone (1) and its metabolites all complied with the Lipinski rule of five, predicted in silico (Table 3). The calculated octanol/water partition coefficient (Log P) and water solubility (Log S) of metabolites 2 − 4 were improved compared to those of 1, especially metabolite 2. These results suggested that the water solubility of the metabolites have been improved relative to the liposoluble substrate.

Table 3
The predicted physicochemical properties of compounds 1 − 4

Compds.	MW	nHBA	nHBD	nRB	Log P	Log S
1	296.36	3	0	0	4.93	−5.10
2	310.34	4	0	0	2.75	−4.05
3	312.39	4	1	0	3.20	−4.18
4	312.39	4	1	0	3.20	−4.18

MW: molecular weight, nHBA: number of acceptor atoms for H-bonds, nHBD: number of donor atoms for H-bonds, nRB: number of rotatable bonds, Log P: octanol/water partition coefficient and Log S: water solubility (log(mol/L)).

4. Discussion

It has been well documented that tanshinones from Chinese traditional medicine Salvia miltiorrhiza Bunge (Danshen) exhibit potential anti-inflammatory activities, like tanshinone IIA, tanshinone I, dihydrotanshinone, and cryptotanshinone[40–43]. They all possess a common active core structure of furanophenanthraquinone. It is hard to make them a direct clinical application due to their high hydrophobicity and poor absorbed property when given orally or intraperitoneally[11]. Sodium tanshinone IIA sulfonate is one of water-soluble derivatives of tanshinone IIA without change of basic skeleton[11].

Biotransformation has been considered as a mild and effective approach to improve the water solubility and activities for natural products[44,45]. In our study, cryptotanshinone was biotransformed by only oxidation at C-3 of its cyclohexane moiety without destruction of the active core. The obtained three oxygenated products thereby possess improved physicochemical properties. Our next work is to dig the effective tool enzymes from Cunninghamella elegans AS3.2028 for further amplified preparation, especially for 2.

Our bioassay results indicated that the three oxygenated products of cryptotanshinone could significantly suppress the LPS-induced production of NO, IL-1β, IL-6 and TNF-α. Excessive NO and proinflammatory cytokines may lead severe diseases such as septic shock, inflammatory diseases and neurotoxicity[31]. Proinflammatory cytokines upregulate both of COX-2 and iNOS expression via the NF-κB or MAPK pathway[46,47]. Compound 2 showed an excellent inhibitory effect on the expression of iNOS and COX-2, which play an important role in the innate response in activated microglia cells. The RNA-seq analysis revealed that LPS could upregulate the transcription levels of lots of inflammatory cytokines in BV-2 cells (Table S1), which mostly enriched in MAPK pathway. MAPK signaling pathway was regarded as an attractive target due to its capability of reducing the synthesis of pro-inflammatory cytokines and their signaling[48]. In MAPK signaling pathway, exogenous LPS was transferred by a lipid exchange molecule, LBP, to its major receptor CD14 on cell membrane. The immediately formed CD14/TLR4 complex plays a vital role in initiating LPS signaling during inflammation. Upon activation of TLR4 with LPS, MyD88 recruits IRAK 4 in cytoplasm and then activate the phosphorylation of IRAK1[49]. Phosphorylated IRAK1 and TRAF6 further motivate the phosphorylation of TAK1[50]. In turn, TAK1 phosphorylates MAPK, eventually resulting in the activation of NF-κB, which plays an important role in the LPS-induced production of pro-inflammatory cytokines (Fig. 8)[51]. In the present study, as shown in Fig. 5, LPS intensely increased the phosphorylation of JNK, ERK and p38 in BV-2 cells. While when cells were pre-treated with compound 2, their phosphorylation levels were significantly decreased. In addition, the immunofluorescence results suggested that compound 2 could also attenuate the action of p65 in the nucleus of LPS-stimulated BV-2 cells (Fig. 6). Thus, compound 2 could relieve the stimulation of LPS to BV-2 cells and downregulate the expression level of TLR4 to influence the downstream signaling and inhibit the production of pro-inflammatory factors to exhibit anti-neuroinflammatory effect (Fig. 8).

Intriguingly, compound 2 also displayed the neuroprotective activities against glutamate-induced oxidative toxicity in HT22 neuronal cells and modest AChE inhibitory activity. These results suggested that 2 could be considered as a promising candidate for development of AD drug. The absorption, bioavailability and metabolism in vivo of 2 need to be further investigated.

5. Conclusions

In conclusion, cryptotanshinone (1), a bioactive constituent from the traditional Chinese medicine, was modified via biotransformation method by the fungus C. elegans AS 3.2028. Three transformed products (2 – 4) were obtained and identified. Compared to the substrate, the bioactivities of the transformed

products were obviously improved, including anti-neuroinflammatory, neuroprotective, and AChE inhibitory activities. Compound 2 exerted anti-neuroinflammatory effects mainly through TLR4/MAPK pathway. The physicochemical properties of the transformed products were also ameliorated. The above results may provide inspiration and possible strategy for the development of cryptotanshinone as a promising candidate to treat AD.

Abbreviations

HRESIMS
High resolution electrospray ionization mass spectroscopy
NMR
Nuclear Magnetic Resonance
ECD
Electron circular dichroism
ELISA
Enzyme linked immunosorbent assay
IL-1β
Interleukin-1 beta
IL-6
Interleukin-6
TNF-α
Tumor necrosis factor alpha
COX-2
Cyclooxygenase-2
iNOS
inducible nitric oxide synthase
TLR4
Toll-likereceptor4
MAPK
Mitogen-activated protein kinase
JNK
c-Jun N-terminal kinase
ERK
Extracellular regulated protein kinases
P38
p38 protein kinases
NF-κB
nuclear factor kappa-B

Declarations

Ethics declarations

Ethics approval and consent to participate

Not applicable

Consent for publication

All the authors have approved the manuscript.

Availability of data and materials

All data generated or analyzed during this study are included in this published article [and its supplementary information files].

Competing interests

The authors declare that they have no competing interests.

Funding

This work was supported by the Marine S&T Fund of Shandong Province for Pilot National Laboratory for Marine Science and Technology (Qingdao, China) (No. 2018SDKJ0406-5), National Science and Technology Major Project for Significant New Drugs Development, China (No. 2018ZX09735-004), the Program of Open Studio for Druggability Research of Marine Natural Products, Pilot National Laboratory for Marine Science and Technology (Qingdao, China) Directed by Kai-Xian Chen and Yue-Wei Guo, and the Taishan Scholars Program, China.

Author contributions

Chang-Yun Wang and Chang-Lun Shao conceived of and proposed the idea. Jing-Shuai Wu and Qin-Yu Meng designed the study. Jing-Shuai Wu, Qin-Yu Meng, Xiao-Hui Shi, and Zhen-Kun Zhang performed the experiments. Jing-Shuai Wu and Qin-Yu Meng participated in data analysis. Chang-Yun Wang, Chang-Lun Shao, and Hua-Shi Guan contributed to writing assistance and proof reading the manuscript. All authors read and approved the final manuscript.

Acknowledgements

Not applicable.

References

1. Du X, Wang X, Geng M. Alzheimer's disease hypothesis and related therapies. *Transl. Neurodegener* 2018;**7**:2.
2. Ahmad SS, Akhtar S, Jamal QMS, Rizvi SMD, Kamal MA, Khan MKA, et al. Multiple targets for the management of Alzheimer's disease. *CNS Neurol. Disord.: Drug Targets* 2016;**15**:1279–1289.
3. Cummings J, Lee G, Ritter A, Sabbagh M, Zhong K. Alzheimer's disease drug development pipeline: 2019. *Alzheimer's Dementia* 2019;**5**:272–293.
4. Wang XY, Sun GQ, Feng T, Zhang J, Huang X, Wang T, et al. Sodium oligomannate therapeutically remodels gut microbiota and suppresses gut bacterial amino acids-shaped neuroinflammation to inhibit Alzheimer's disease progression. *Cell Res* 2019;**29**:787–803.
5. Calsolaro V, Edison P. Neuroinflammation in Alzheimer's disease: current evidence and future directions. *Alzheimer's Dementia* 2016;**12**:719–732.
6. Bronzuoli MR, Iacomino A, Steardo L, Scuderi C. Targeting neuroinflammation in Alzheimer's disease. *J. Inflammation Res* 2016;**9**:199.
7. Regen F, Hellmann-Regen J, Costantini E, Reale M. Neuroinflammation and Alzheimer's disease: implications for microglial activation. *Curr. Alzheimer Res* 2017;**14**:1140–1148.
8. Ising C, Heneka MT. Functional and structural damage of neurons by innate immune mechanisms during neurodegeneration. *Cell Death Dis* 2018;**9**:1–8.
9. Shal B, Ding W, Ali H, Kim YS, Khan S. Anti-neuroinflammatory potential of natural products in attenuation of Alzheimer's disease. *Front. Pharmacol* 2018;**9**:548.
10. Wei WJ, Zhou PP, Lin CJ, Wang WF, Li Y, Gao K. Diterpenoids from *Salvia miltiorrhiza* and their immune-modulating activity. *J. Agric. Food Chem* 2017;**65**:5985–5993.
11. Zhang Y, Jiang PX, Ye M, Kim SH, Jiang C, Lü JX. Tanshinones: sources, pharmacokinetics and anti-cancer activities. *Int. J. Mol. Sci* 2012;**13**:13621–13666.
12. Shang Q, Xu H, Huang L. Tanshinone IIA: a promising natural cardioprotective agent. *J. Evidence-Based Complementary Altern. Med* 2012;**2012**:1–5.
13. Zhang XZ, Qian SS, Zhang YJ, Wang RQ. *Salvia miltiorrhiza*: a source for anti-Alzheimer's disease drugs. *Pharm. Biol* 2016;**54**:18–24.
14. Zheng J, Yu X, Wang Q. Tashinones and their derivatives: novel excellent drugs for Alzheimer disease. U.S. Patent Application 2016;**14/773**:536.
15. Tung NH, Nakajima K, Uto T, Hai NT, Long DD, Ohta T, et al. Bioactive triterpenes from the root of *Salvia miltiorrhiza* Bunge. *Phytother. Res* 2017;**31**:1457–1460.
16. Yu XY, Lin SG, Chen X, Zhou ZW, Liang J, Duan W, et al. Transport of cryptotanshinone, a major active triterpenoid in *Salvia miltiorrhiza* Bunge widely used in the treatment of stroke and Alzheimer's disease, across the blood-brain barrier. *Curr. Drug Metab* 2007;**8**:365–377.
17. Hu LD, Xing Q, Meng J, Shang C. Preparation and enhanced oral bioavailability of cryptotanshinone-loaded solid lipid nanoparticles. *AAPS Pharmscitech* 2010;**11**:582–587.

18. Huang WG.; Jiang YY, Li Q, Li J, Li JY, Lu W, et al. Synthesis and biological evaluation of (±)-cryptotanshinone and its simplified analogues as potent CDC25 inhibitors. *Tetrahedron* 2005;**61**:1863–1870.
19. Li MM, Xia F, Li CJ, Xu G, Qin HB. Design, synthesis and cytotoxicity of nitrogen-containing tanshinone derivatives, *Tetrahedron Lett* 2018;**59**:46–48.
20. He WN, Li Y, Qin YJ, Tong XM, Song ZJ, Zhao Y, et al. New cryptotanshinone derivatives with anti-influenza A virus activities obtained via biotransformation by *Mucor rouxii*. *Appl. Microbiol. Biotechnol* 2017;**101**:6365–6374.
21. Sun JH, Yang M, Ma XC, Kang J, Han J, Guo D. A. Microbial biotransformation of cryptotanshinone by *Cunninghamella elegans* and its application for metabolite identification in rat bile. *J. Asian Nat. Prod. Res* 2009;**11**:482–489.
22. Asha S, Vidyavathi M. *Cunninghamella* – A microbial model for drug metabolism studies – A review. *Biotechnol. Adv* 2009;**27**:16–29.
23. Zhang D, Evans FE, Freeman JP, Yang YF, Deck JN, Cerninglia CE. Formation of mammalian metabolites of cyclobenzaprine by the fungus, *Cunninghamella elegans*. *Chem.-Biol. Interact* 1996; **102**:79–92.
24. Xia WJ, Luo P, Hua P, Peng P, Li CJ, Xu J, et al. Discovery of a new pterocarpan-type antineuroinflammatory compound from *Sophora tonkinensis* through suppression of the TLR4/NFκB/MAPK signaling pathway with PU. 1 as a potential target. *ACS Chem. Neurosci* 2018;**10**:295–303.
25. Lee SY, Ahn SM, Wang ZY, Choi YW, Shin HK, Choi BT. Neuroprotective effects of 2,3,5,4'-tetrahydoxystilbene-2-O-β-D-glucoside from *Polygonum multiflorum* against glutamate-induced oxidative toxicity in HT22 cells, *J. Ethnopharmacol* 2017;**195**:64–70.
26. Ellman GL, Courtney KD, Andres JV, Featherstone RM. A new and rapid colorimetric determination of acetylcholinesterase activity. *Biochem. Pharmacol* 1961;**7**:88–95.
27. Teles APC, Takahashi JA. Paecilomide, a new acetylcholinesterase inhibitor from *Paecilomyces lilacinus*. *Microbiol. Res* 2013;**168**:204–210.
28. Janicka M, Sztanke M, Chromatogr K. Reversed-phase liquid chromatography with octadecylsilyl, immobilized artificial membrane and cholesterol columns in correlation studies with in silico biological descriptors of newly synthesized antiproliferative and analgesic active compounds. *J. Chromatogr. A* 2013;**1318**:92–101.
29. Kolios G, Valatas V, Ward SG. Nitric oxide in inflammatory bowel disease: a universal messenger in an unsolved puzzle. *Immunology* 2004;**113**:427–437.
30. Tang S, Shen XY, Huang HQ, Xu SW, Yu Y, Zhou CH, et al. Cryptotanshinone suppressed inflammatory cytokines secretion in RAW264.7 macrophages through inhibition of the NF-κB and MAPK signaling pathways. *Inflammation* 2011;**34**:111–118.
31. Li X, Lian LH, Bai T, Wu YL, Wan Y, Xie WX, et al. Cryptotanshinone inhibits LPS-induced proinflammatory mediators via TLR4 and TAK1 signaling pathway. *Int. Immunopharmacol*

2011;**11**:1871–1876.

32. Cao SG, Chen RJ, Wang H, Lin LM, Xia XP. Cryptotanshinone inhibits prostaglandin E2 production and COX-2 expression via suppression of TLR4/NF-κB signaling pathway in LPS-stimulated Caco-2 cells. *Microb. Pathog* 2018;**116**:313–317.
33. Lee P, Hur J, Lee J, Kim J, Jeong J, Kang I, et al. 15,16-Dihydrotanshinone I suppresses the activation of BV-2 cell, a murine microglia cell line, by lipopolysaccharide. *Neurochem. Int* 2006;**48**:60–66.
34. Watkins LR, Maier SF, Goehler LE. Immune activation: the role of pro-inflammatory cytokines in inflammation, illness responses and pathological pain states. *Pain* 1995;**63**:289-302.
35. Chan KL Wong KF, Luk JM. Role of LPS/CD14/TLR4-mediated inflammation in necrotizing enterocolitis: pathogenesis and therapeutic implications. *World J. Gastroenterol* 2009;**15**:4745.
36. Choi DW. Glutamate neurotoxicity and diseases of the nervous system. *Neuron* 1988;**1**:623–634.
37. Kroplewska KS, Wrońska A, Stasiłojć G, Kmieć Z. The designer drug 3-fluoromethcathinone induces oxidative stress and activates autophagy in HT22 neuronal cells. *Neurotoxic. Res* 2018;**34**:1–13.
38. Dixon SJ, Stockwell BR. The role of iron and reactive oxygen species in cell death. *Nat. Chem. Biol* 2014;**10**:9–17.
39. Vilela AFL, Cardoso CL, Mateo C. An immobilized acetylcholinesterase as test system to screen new inhibitor drugs to treat Alzheimer's disease. *Sens. Actuators, B* 2019;**278**:196–201.
40. Choi HS, Cho DI, Choi HK, Im SY, Ryu, S. Y, Kim KM. Molecular mechanisms of inhibitory activities of tanshinones on lipopolysaccharide-induced nitric oxide generation in RAW264.7 cells. *Arch Pharm Res* 2004;**27**:1233–1237.
41. Jang SI, Kim KJ, Kim HJ, Yu HH, Park R, Kim HM, et al. Tanshinone IIA from *Salvia miltiorrhiza* inhibits inducible nitric oxide synthase expression and production of TNF-α, IL-1β and IL-6 in activated RAW 264.7 cells. *Planta Med* 2003;**69**:1057–1059.
42. Jeon SJ, Son KH, Kim YS, Choi YH, Kim HP. Inhibition of prostaglandin and nitric oxide production in lipopolysaccharide-treated RAW264.7 cells by tanshinones from the roots of *Salvia miltiorrhiza* Bunge. *Arch Pharm Res* 2008;**31**:758–763.
43. Kang BY, Chung SW, Kim SH, Ryu SY, Kim TS. Inhibition of interleukin-12 and interferon-γ production in immune cells by tanshinones from *Salvia miltiorrhiza*. *Immunopharmacology* 2000;**49**:355–361.
44. Yao H, Liu JK, Xu ST, Zhu ZY, Xu JY. The structural modification of natural products for novel drug discovery. *Expert Opin. Drug Discovery* 2017;**12**:121–140.
45. Liu JH, Yu BY. Biotransformation of bioactive natural products for pharmaceutical lead compounds. *Curr. Org. Chem* 2010;**14**:1400–1406.
46. West AP, Koblansky AA, Ghosh S. Recognition and signaling by toll-like receptors. *Annu. Rev. Cell Dev. Biol* 2006;**22**:409–437.
47. Shabab T, Khanabdali R, Moghadamtousi SZ, Kadir HA, Mohan G. Neuroinflammation pathways: a general review. *Int. J. Neurosci* 2017;**127**:624–633.

48. Yeung YT, Aziz F, Guerrero-Castilla A, Arguelles S. Signaling pathways in inflammation and anti-inflammatory therapies. *Curr. Pharm. Des* 2018;**24**:1449–1484.
49. Yamamoto M. Role of adaptor TRIF in the MyD88-independent toll-like receptor signaling pathway. *Science* 2003;**301**:640–643.
50. Kagan JC, Medzhitov R. Phosphoinositide-mediated adaptor recruitment controls Toll-like receptor signaling. *Cell* 2006;**125**:943–955.
51. Min S, More SV, Park JY, Jeon SB, Park SY, Park EJ, et al. EOP, a newly synthesized ethyl pyruvate derivative, attenuates the production of inflammatory mediators via p38, ERK and NF-κB pathways in lipopolysaccharide-activated BV-2 microglial cells. *Molecules* 2014;**19**:19361–19375.

Figures

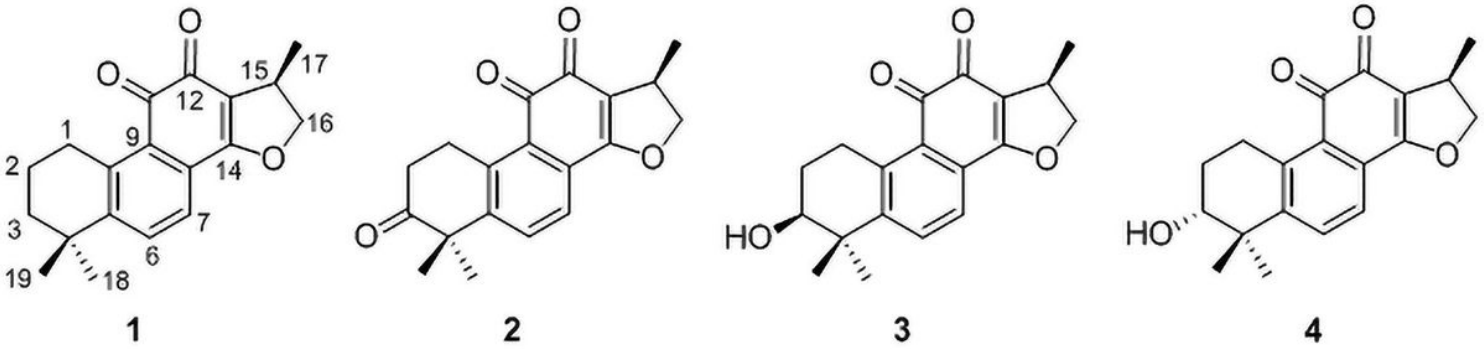

Figure 1

Structures of cryptotanshinone (1) and its biotransformed products (2–4).

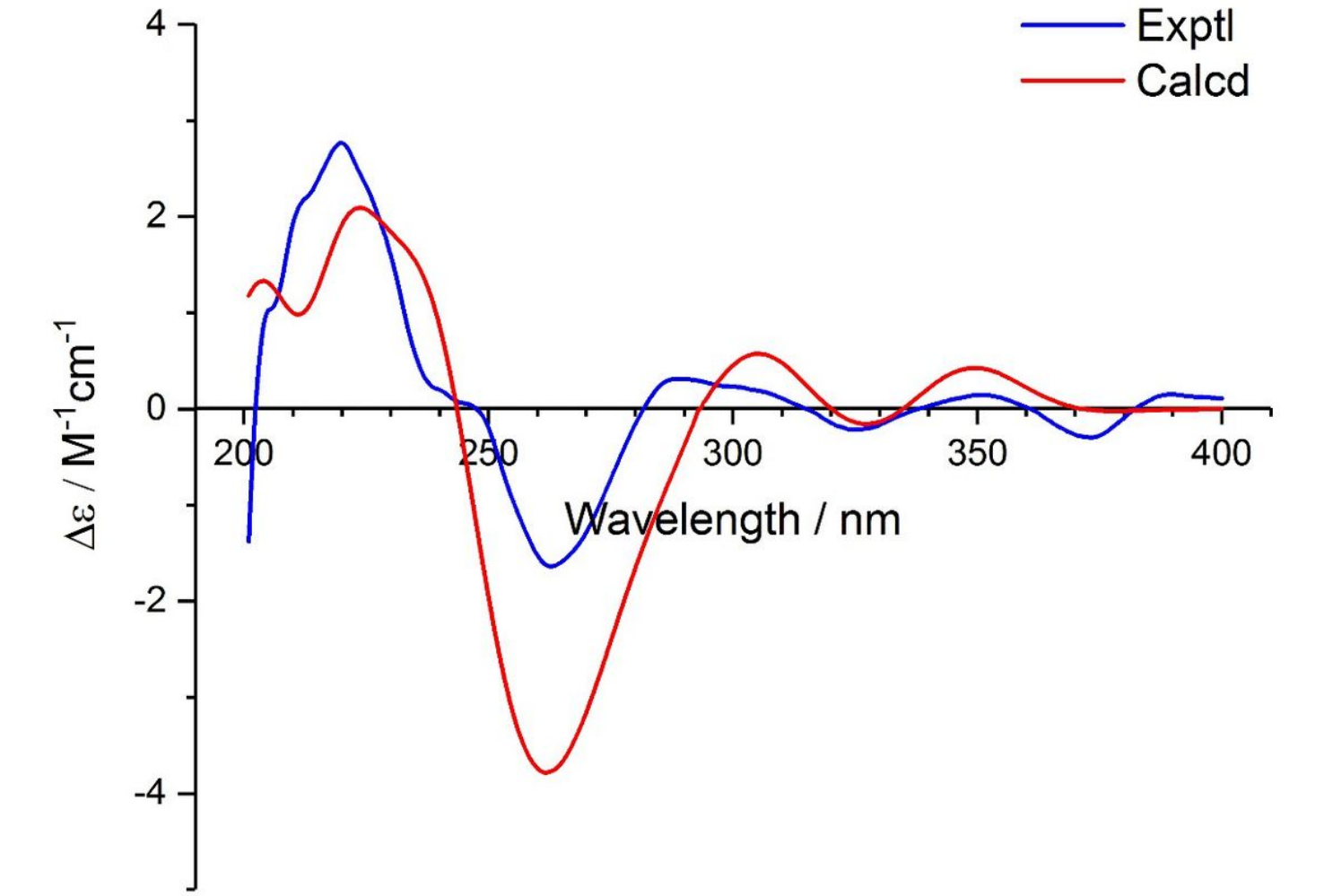

Figure 2

Experimental and calculated ECD spectra of 2.

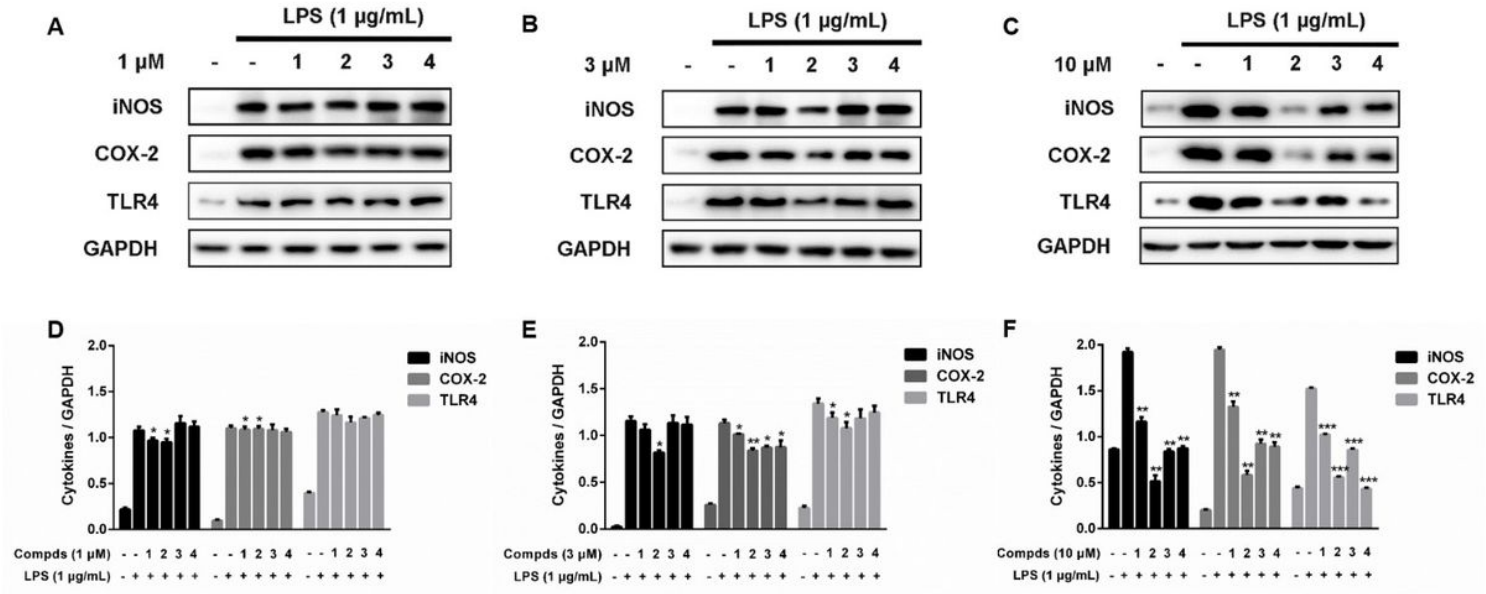

Figure 3

. Effects of compounds 1–4 on cytokines expression of iNOS, COX-2 and TLR4 in LPS-stimulated BV-2 cells by Western blot. (A, B, C) The levels of cytokines in BV-2 cells are shown as the relative change at the concentrations of 1, 3, and 10 μM in comparison to the LPS treatment. (D, E, F) Densitometric analyses of the expressed cytokines to GAPDH. Data are the mean ± standard error of three independent experiments. *p < 0.05, **p < 0.01, ***p < 0.001, compared with the LPS-treated group.

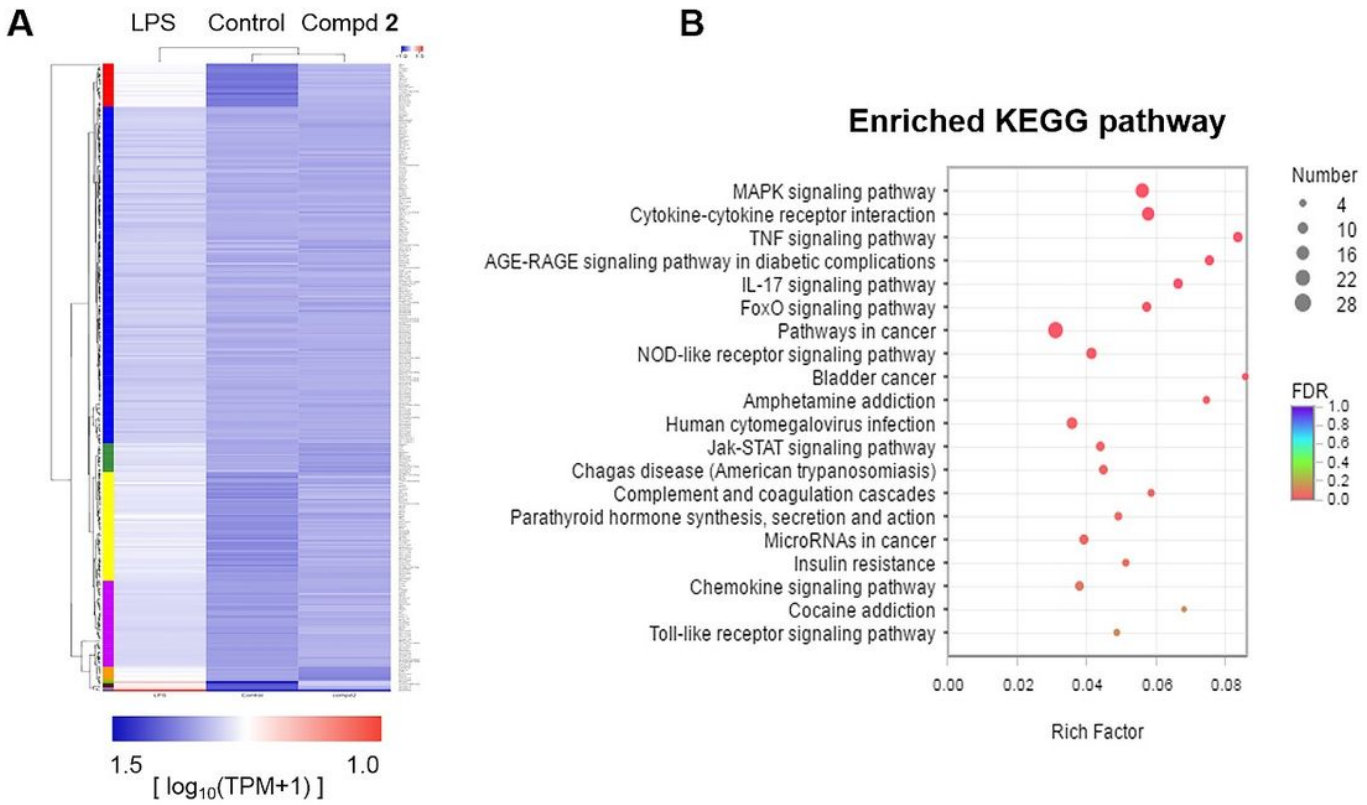

Figure 4

The potential pathway and mechanism of compound 2 revealed by RNA-seq analysis. (A) Differentially expressed genes (DEGs) of BV-2 cells treated by compound 2. Red in the heat-map indicates high expression, white denotes medial expression, and blue indicates low expression. (B) Functional enrichment analysis of the KEGG pathway.

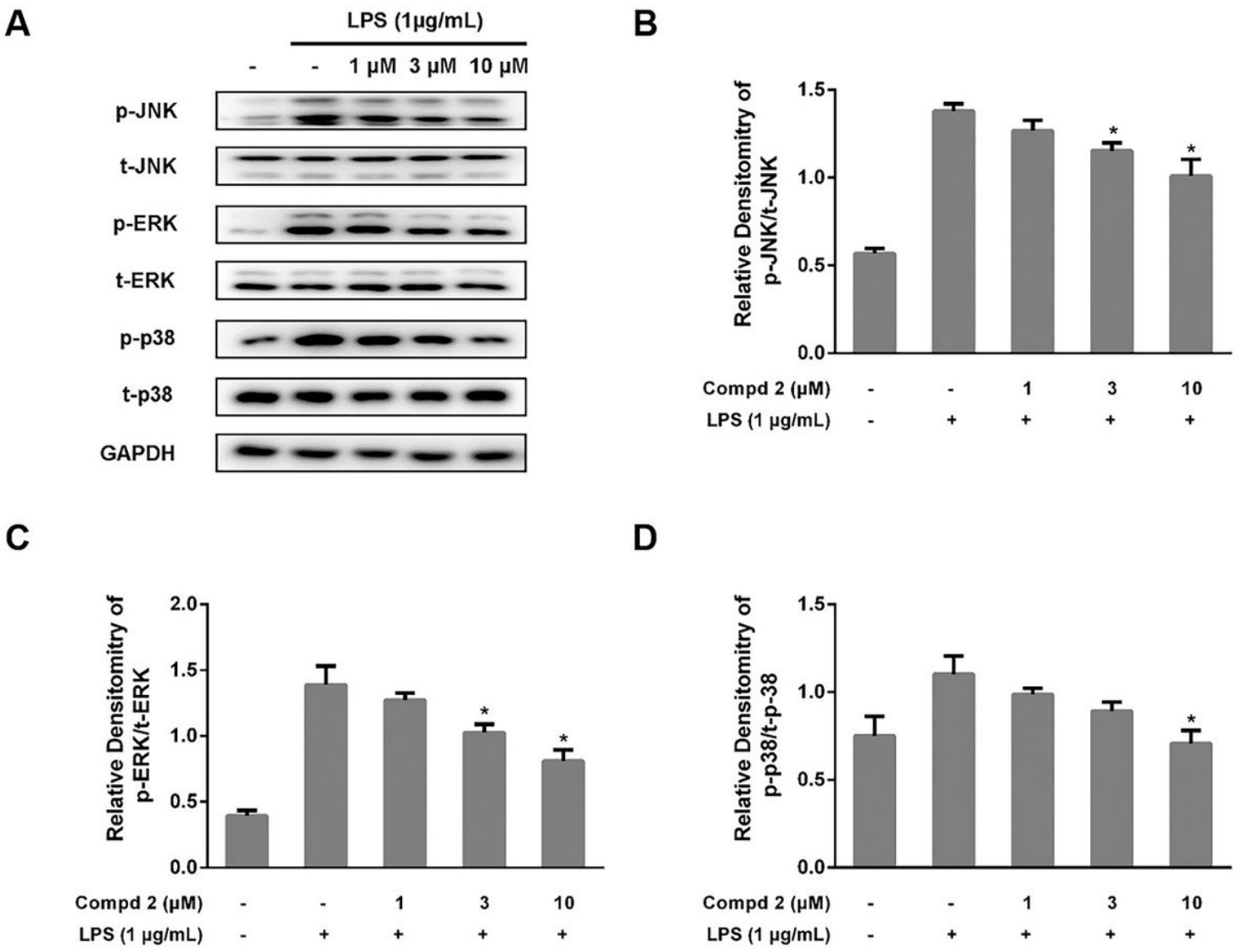

Figure 5

The phosphorylation detection of JNK, ERK, and p38 influenced by compound 2 in LPS-stimulated BV-2 cells by Western blot. (A) The levels of phospho-JNK, ERK, and p38 in BV-2 cells expressed as a relative change in comparison to their total protein fragments. (B, C, D) Densitometric analyses of phospho-JNK, ERK, and p38. Data are the mean ± standard error of three independent experiments. *p < 0.05, **p < 0.01, ***p < 0.001, compared with the LPS-treated group.

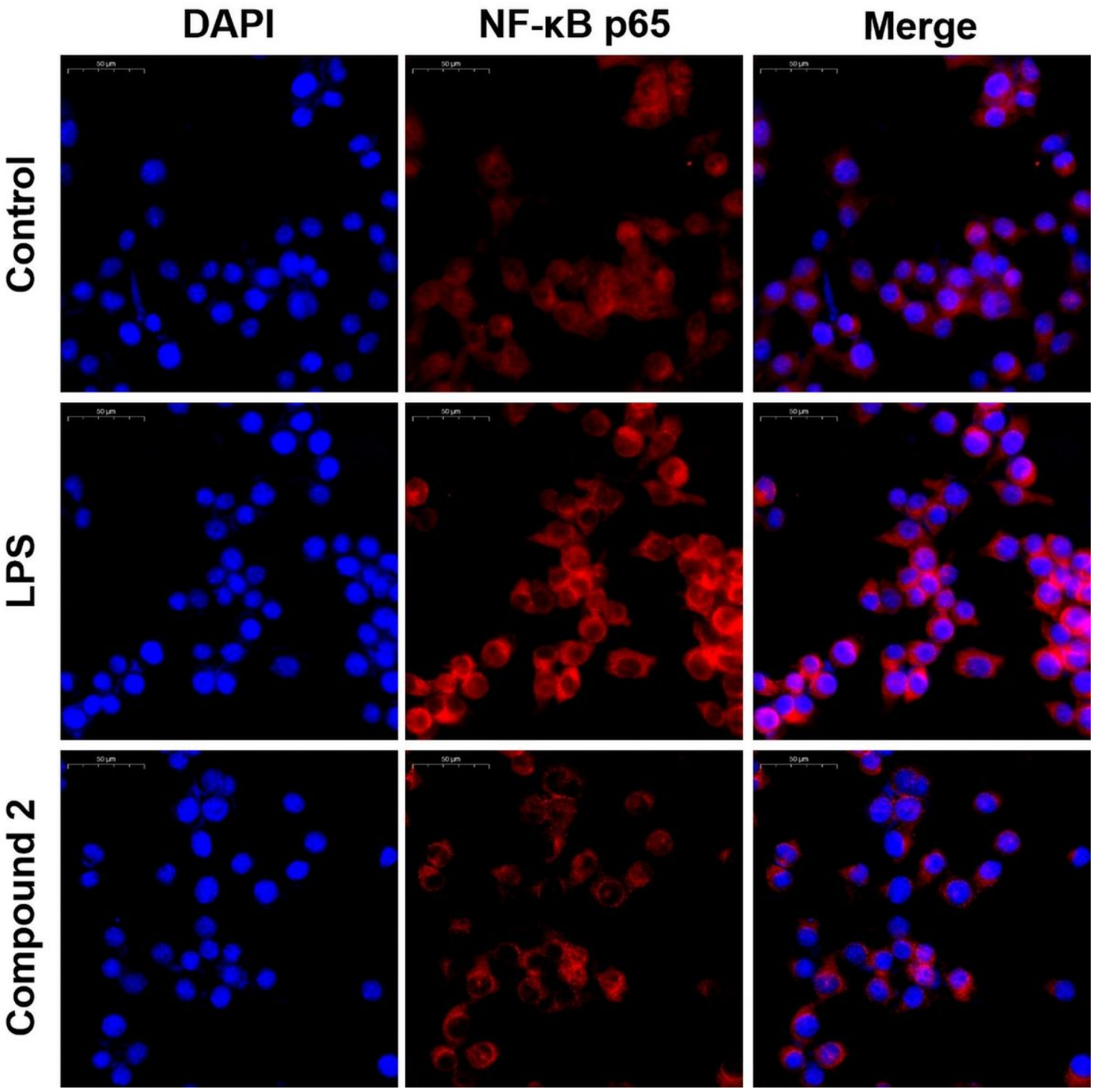

Figure 6

The effects of compound 2 on the nuclear translocation of NF-κB p65 in LPS-stimulated BV2 cells. Immunofluorescence staining detected the distribution of NF-κB p65 by the colocalization of receptors (p65, red) with nuclei (DAPI, blue).

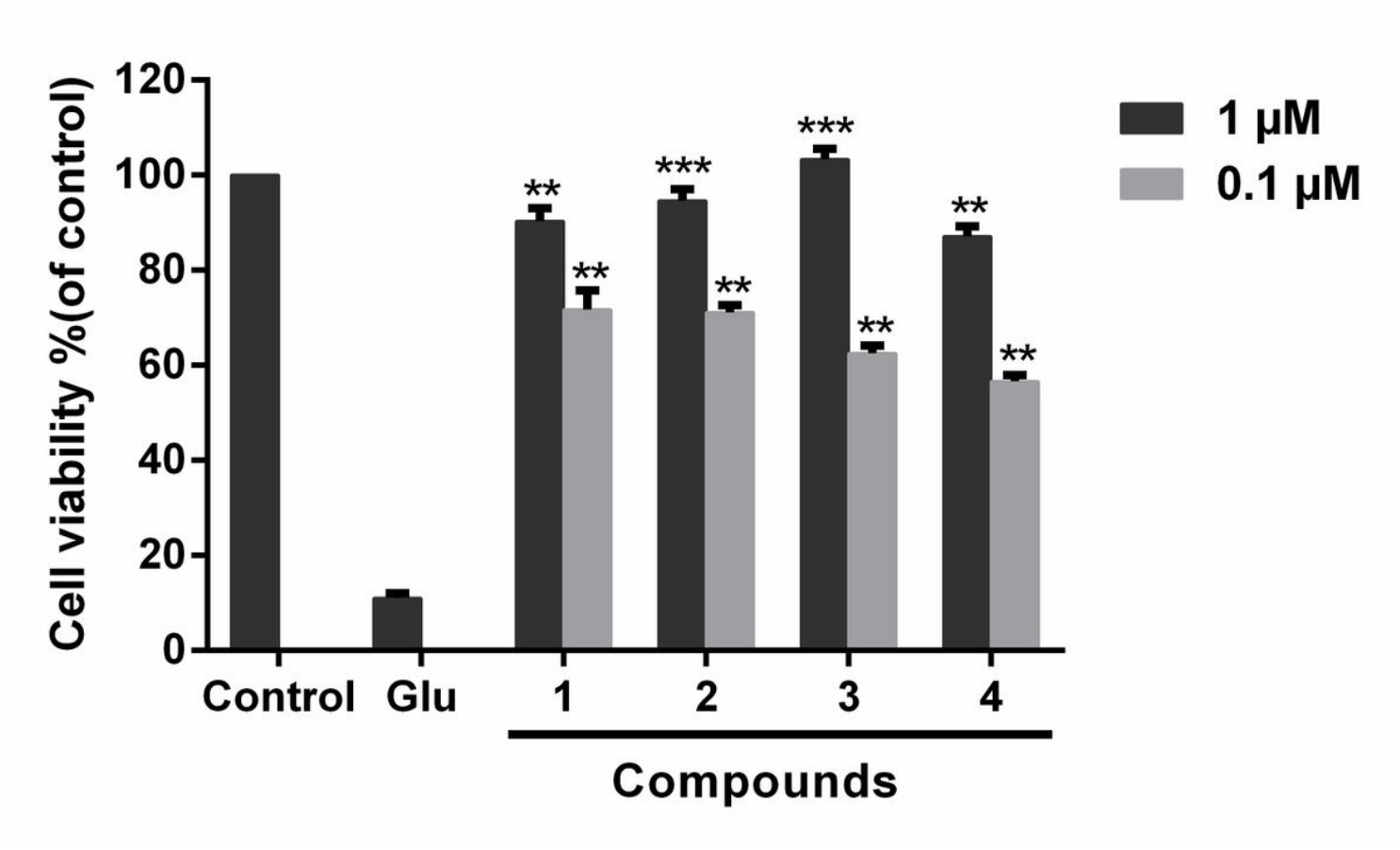

Figure 7

Neuroprotective activities of compounds 1–4 against glutamate-induced HT22 neuronal cell death. The cell viability after treating with 5 mM glutamate in the presence or absence of compounds. Data are the mean ± standard error of three independent experiments. *p < 0.05, **p < 0.01, ***p < 0.001 compared with the Glu-treated group.

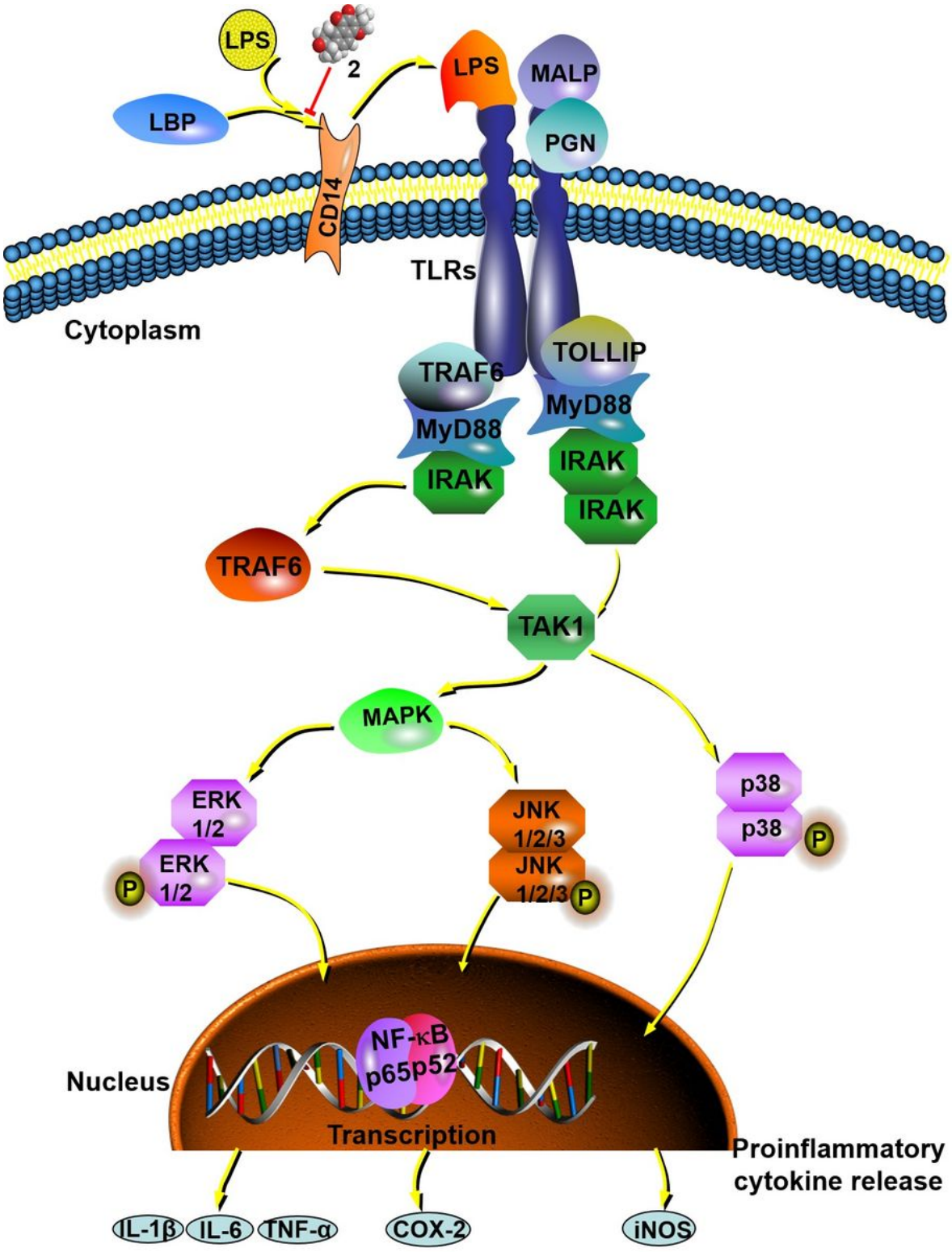

Figure 8

The proposed signaling mechanism for the inhibitory effects of compound 2 on LPS stimulated neuroinflammation in BV2 cells.

Supplementary Files

This is a list of supplementary files associated with this preprint. Click to download.

- Additionalfile1.docx
- Additionalfile2.xls